RESEARCH ARTICLE | JUNE 19 2020

Structured channel metamaterials for deep sub-wavelength resolution in guided ultrasonics

Special Collection: 2020 Materials Science

John K. Birir; Michael J. Gatari; Prabhu Rajagopal

+ Author & Article Information

AIP Advances 10, 065027 (2020)

https://doi.org/10.1063/1.5143696 **Article history**

Experimental results on deep subwavelength resolution of defects are presented for the first time in the context of guided ultrasonic wave inspection of defects, using novel “structured channel” metamaterials. An Aluminum bar with side-drilled holes is used as a test sample, interrogated by the fundamental bar-guided symmetric mode. Simulations were conducted to optimize dimensional parameters of the metamaterial structure. Experiments using metamaterials fabricated accordingly demonstrate a resolution down to 1/72 of the operating wavelength, potentially bringing the resolution of guided wave inspection to the same range as that of bulk ultrasonics. This work has much promise for remote inspection in industry and biomedicine.

Guided ultrasonic waves are of much interest to non-invasive imaging and material diagnostics as they provide the ability to inspect structures from a remote location up to several meters.[1,2] Today, guided waves find wide use in biomedical diagnostics[3,4] and in internal assessments of composites[5] and concrete[6,7] both during setting and operational lifetime. Waveguide sensors also permit remote monitoring under challenging conditions such as high temperature and radiation[8,9] as well as the possibility for mediation in the micro-nanoscale.[10,11]

Inspection methods are diffraction-limited, and the best resolution achievable is λ/2, where λ is the operating wavelength.[12] For guided ultrasonic waves,[13] especially at lower frequencies, λ is in the order of several centimeters, and hence, resolution is relatively poorer compared to even bulk ultrasound, not to speak of electromagnetic wave-based methods. Due to this limitation, guided waves are primarily used as a long-range screening tool. A secondary localized method is then employed in the identified area of interest for a detailed characterization of defect features. Improving the resolution of guided wave

inspections is, thus, of much interest, impacting novel sensing methods across engineering and biomedicine.

In recent years, metamaterials have been shown to overcome diffraction limitations in fields such as optics and acoustics, where they have been shown to yield a resolution of several orders of magnitude below λ.[14–16] Recently, work by the authors at IIT-Madras has yielded several types of holey structured metamaterial concepts for applications in bulk ultrasonics.[17–20] Here, for the first time, we experimentally demonstrate a novel metamaterial concept to achieve sub-wavelength super-resolution in guided ultrasonics.

With the use of metamaterials, evanescent waves can be amplified and transmitted, thus improving the resolution of smaller features.[12,17–21] To achieve super-resolution, three techniques have been discussed in the literature, namely, near-field imaging,[22] negative index media,[23] and resonating structures.[12,17,18,21,24] For the work reported in this paper, resonating structures were designed and developed for achieving the intended goal

of super-resolution imaging as this approach is convenient to realize and cost-effective to fabricate.

The detection concept investigated here is shown in **Fig. 1**. The metamaterial structure proposed here for use in guided wave applications consists of a series of “channels” arranged periodically. With proper selection of channel size, length, and periodicity, Fabry–Pérot resonances[17] can be used to magnify and transmit evanescent waves arising from scattering by a defect.

FIG. 1.

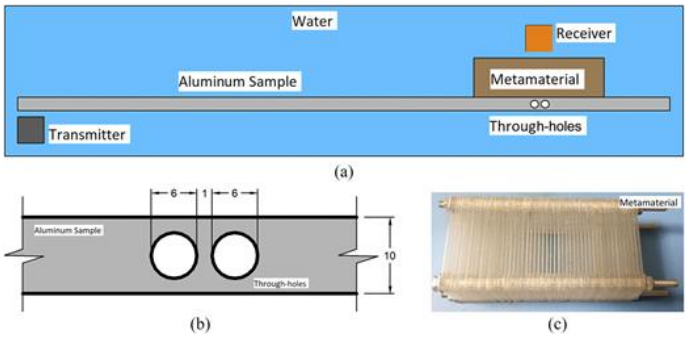

(a) Illustration of the detection concept investigated here. (b) Details of the through-holes in the aluminum bar sample used for the experiments. (c) Photograph of the channel structured metamaterial proposed in this paper.

The transmission coefficient for a plane wave can be written as[12]

$$T(\lambda, m) = \frac{4\left(\frac{a}{\Lambda}\right)^2 Y e^{ikl}}{\left(1+Y\left(\frac{a}{\Lambda}\right)^2\right)^2 - \left(1-Y\left(\frac{a}{\Lambda}\right)^2\right)^2 e^{2ikl}}, \quad (1)$$

where $Y = \frac{k}{\sqrt{k^2-m^2}}$, m = $\sqrt{\left({k_x}^2 + {k_x}^2\right)}$, k = $\frac{2\pi}{\lambda}$, *a* is the size of the metamaterial channel, *l* is the length of the metamaterial, *Λ* is the size of the unit cell (periodicity), *k* is the propagation constant, and *m* is the parallel momentum.

It can be noted from Eq. (1) that for the resonance condition, *kl* = *nπ*, where *n* is an

integer.

Finite element (FE) simulations were used to select and optimize variables in the construction of the structured channel metamaterial. The specimen sample to be inspected is taken to be an aluminum bar with two circular cylindrical side-drilled through-holes. At the center of the bar, this can be well represented by a two-dimensional (2D) plane strain approximation. In the work reported here, the fundamental symmetric Lamb mode S0 was selected for the studies, operating at 0.75 MHz-mm. By choosing a bar of thickness 10 mm, the frequency is fixed at 75 kHz. The wavelength (λ) at this frequency is fairly large at ~72 mm.

A sample plate of 1 m length and 10 mm thickness is modeled in 2D. The plate has two circular holes each of 6 mm diameter (λ/12) and separated by 1 mm (this is about λ/72 at the 75 kHz used for excitation). Both the holes are assumed to be centered on the axis of the plate, bisecting it thickness-wise. Channels were built into the water matrix by creating empty spaces of specified dimensions. Simulations were performed to optimize the

dimensions of these channels, namely, length, size, and pattern. The work reported in this paper is based on a metamaterial of 30 mm length, channel of 1 mm size, and pattern unit cell (periodicity) of 2 mm. For purposes of comparison, simulations were performed with and without the use of the metamaterial.

Simulations were performed using a commercial FE package (**https://www.3ds.com**) in the explicit time-domain regime. The part was modeled as a two-dimensional (2D) deformable shell. The mesh for the sample consisted of 4-node bilinear plane-strain quadrilateral elements of size 0.2 mm (λ/360 in aluminum), while water was modeled using 4-node linear, 2D acoustic quadrilateral elements. A Hanning windowed 3-cycle pulse[19] centered at the frequency of 75 kHz was used for excitation.

Amplitudes were recorded at a line of nodes located above the defect for two scenarios, with and without the structured channel metamaterial lens, with the results shown in **Fig. 2** (experimental results are also presented, which will be discussed later). In simulations, the pressure amplitudes were recorded on the

water side of the model, as illustrated in Fig. 1(a). In experiments, the “out-of-plane” displacement amplitudes were recorded using a fiber-optic laser Doppler vibrometer (details of the experimental setup are given in the following paragraph). For the case without the metamaterial, it can be seen that the defects are not detected (see Fig. 2). This is to be expected since the defect is much smaller than λ/2. Therefore, it is not possible to resolve the two defects without some form of intervention. In the second case, the defects can be clearly resolved due to the evanescent components being recovered by the channel metamaterial (see, e.g., Refs. 17 and 20).

FIG. 2.

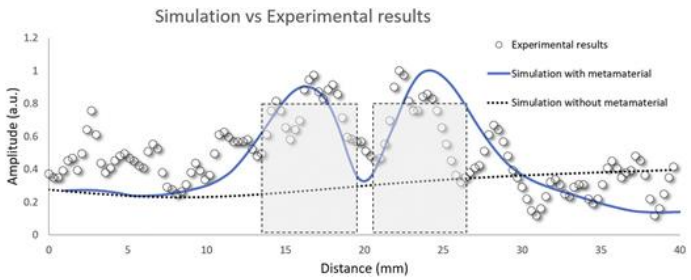

Experimental results for two defects spaced λ/72 apart (see shaded rectangles) imaged with metamaterial, overlaid with simulation results.

These results were then experimentally verified using a channel metamaterial fabricated as per guidance from simulation studies. A longitudinal bulk ultrasonic probe (Panametrics NDT) was used to obtain the S0 wave excitation at the central frequency of 75 kHz. A flat aluminum bar of 1 m length, 50 mm width, and 10 mm thickness was selected, and two circular through-holes of 6 mm diameter and separated by 1 mm (λ/72) were side-drilled on this sample. The phase velocity of S0 guided waves in aluminum was measured to be 5413 m/s [the wavelength (λ) is thus determined to be about 72 mm]. Using Snell's law, the incident angle of excitation was determined to be 15.9° in order to generate the desired mode in the plate through water.

Figure 1 shows a photograph of the metamaterial used and an illustration of how it was located on the sample relative to the defect position. Figure 3 presents a photograph of the actual experimental setup, showing different equipment used, the sample, and their relative positions.

FIG. 3.

Photograph of the (a) experimental setup and (b) transmitter, sample, and receiver position.

The sample, metamaterial, and probe were immersed in water to ensure proper coupling between the probe and the sample and to create flexibility in probe angle manipulation for the purpose of generating the desired S0 guided wave mode. A fiber-optic laser Doppler vibrometer (OFV 551, Polytec GmbH, Germany, https://www.polytec.com) controlled by using a laser controller (OFV 5000, Polytec) was used as the receiver to record out-of-plane displacements. The

electronic controls were performed using Ritec RPR-4000 pulser-receiver (Ritec Inc., http://www.ritecinc.com, Warwick, USA). The display oscilloscope (National Instruments, USB-5132, 50 MHz bandwidth, 2-channel, 8-bit USB oscilloscope device, http://www.ni.com), the transmitter (piezoelectric probe), and the receiver (laser vibrometer) were connected through the Ritec RPR-4000 pulser-receiver. A 3-cycle pulse was generated from the controller, driving the transducer at 75 kHz.

The results from experiments are shown in Fig. 2, overlaid with the simulation results—we find that the proposed structured channel metamaterial lens is able to resolve defects way smaller than the operating wavelength. Based on the relative positions of the transmitter, the receiver, and the defects, the clear signals seen in the results can be attributed to diffractions from the circular hole defects. As the incident wave hits the reflector (holes), part of the signal is diffracted in the perpendicular direction. It is this diffracted signal that is being picked by the sensors in those positions.

To evaluate how signals varied with changes in hole diameter, simulations were conducted for various holes ranging from 3 mm (λ/24) to 9 mm (λ/8). **Figure 4** shows results for 3 mm, 6 mm, and 9 mm hole cases. In each case, the separation between the holes is fixed at λ/72. It was observed that hole diameters less than 6 mm could not be resolved. However, for separation ≥6 mm, two peaks coinciding with the position of the holes can be observed. This resolution is for the specific metamaterial configuration and dimensions used in this work. Ongoing work by the group is to further optimize the metamaterial dimensions to achieve better resolution for holes less than 6 mm diameter for the same configuration.

FIG. 4.

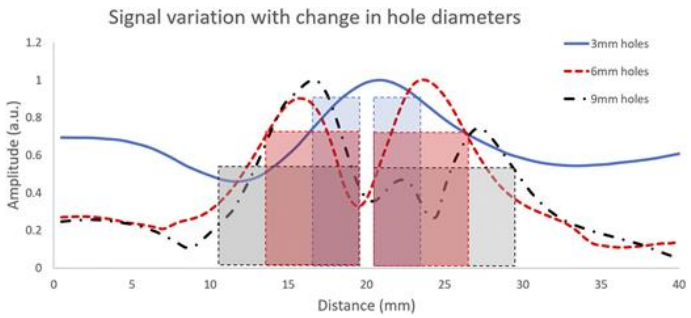

FE simulation results for signal variation with a change in hole diameter for a separation of λ/72 for 3 mm, 6 mm, and 9 mm hole cases.

FE simulation studies were also conducted for different hole diameters for separations ranging from several wavelengths (λ) to fractions of a wavelength. There was consistency for various hole sizes. In this paper, we report results for 4 mm holes [Fig. 5(a)] and 6 mm holes [Fig. 5(b)]. For clarity, we plot the results for a hole separation of λ/36, λ/9, and λ/2 for 4 mm holes, while for 6 mm holes, we plot for λ/72, λ/9, and λ/2. (These three cases represent the scenarios where the hole separation is far lower and in the range of λ/2.) We note from Figs. 5(a) and 5(b) that in the case of 4 mm holes, the resolution is achieved up to a separation of λ/9, while for 6 mm holes, resolution is achieved up to λ/72. This

resolution varies for the various hole sizes. Further work is ongoing to optimize the setup and metamaterials as indicated above to achieve improved resolution for smaller defect sizes and separation distances.

FIG. 5.

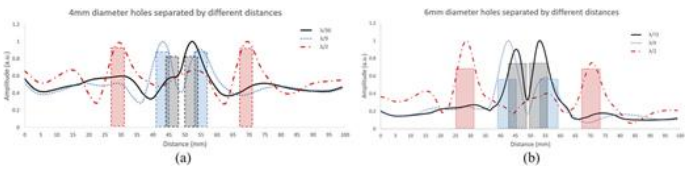

FE simulation results for signal variation with hole separation distance for (a) 4 mm holes and (b) 6 mm holes.

This paper presents the first experimental demonstration of super-resolution and sub-wavelength imaging beyond the diffraction limit in guided ultrasonic wave inspection, using novel structured channel metamaterials as proposed by the authors. The resolution of $\lambda/72$ as reported here is also the highest ever resolution reported in the ultrasonic regime. This work offers avenues for novel guided wave applications in inspection of critical assets from a remote location. Ongoing work

includes expanding this to different sizes and geometries of defects.

DATA AVAILABILITY

The data that support the findings of this study are available from the corresponding author upon reasonable request.

P.R. would like to acknowledge support from the IIT Madras New Faculty Seed Grant. A University of Nairobi-IIT Madras Ph.D. joint-degree programme and MoU and Grant support to Institute of Nuclear Science and Technology by International Science Programme, enabled J.K.B. to travel to IIT Madras to study and conduct experiments. IIT Madras supported stay, studies and research while ISP Supported flights and Nairobi visits by P.R. The grant also supported conference attendance in US besides the facilities in INST, UON, Kenya.

REFERENCES

1. M. Mitra and S. Gopalakrishnan, *Smart Mater. Struct.* 25, 053001 (2016).

https://doi.org/10.1088/0964-1726/25/5/053001
Google Scholar Crossref

2. R. S. Panda, P. Rajagopal, and K. Balasubramaniam, *Compos. Struct.* 206, 247–260 (2018).
https://doi.org/10.1016/j.compstruct.2018.08.024
Google Scholar Crossref

3. D. R. Thakare, A. Abid, D. Pereira, J. Fernandes, P. Belanger, and P. Rajagopal, *Int. Biomech.* 4, 17 (2017).
https://doi.org/10.1080/23335432.2017.1319295
Google Scholar Crossref

4. J. Schneider, D. Ramiandrisoa, G. Armbrecht, Z. Ritter, D. Felsenberg, K. Raum, and J.-G. Minonzio, *Ultrasound Med. Biol.* 45(5), 1234–1242 (2019).
https://doi.org/10.1016/j.ultrasmedbio.2019.01.008
Google Scholar Crossref
PubMed

5. S. Gupta and P. Rajagopal, *Ultrasonics* 90, 109–119 (2018).
https://doi.org/10.1016/j.ultras.2018.06.007
Google Scholar Crossref
PubMed

6. H. Mohseni and C.-T. Ng, *Struct. Health Monit.* 18(1), 303–317 (2019).

https://doi.org/10.1177/1475921718754371
Google Scholar Crossref

7. P. Giri, S. Kharkovsky, X. Zhu, S. M. Clark, and B. Samali, *Struct. Health Monit.* 28, 045020 (2019).
https://doi.org/10.1088/1361-665x/ab0b6e
Google Scholar Crossref

8. A. A. Jacob, P. Rajagopal, and K. Balasubramaniam, *NDT&E Int.* 94, 47–55 (2018).
https://doi.org/10.1016/j.ndteint.2017.11.005
Google Scholar Crossref

9. S.-b. Oh, Y.-m. Cheong, D.-j. Kim, and K.-m. Kim, *Sensors* 19(8), 1762 (2019).
https://doi.org/10.3390/s19081762
Google Scholar Crossref
PubMed

10. V. I. Anisimkin and I. E. Kuznetsova, *J. Commun. Technol. Electron.* 64(8), 823–826 (2019).
https://doi.org/10.1134/s1064226919080011
Google Scholar Crossref

11. C. Caliendo and M. Hamidullah, *J. Phys. D: Appl. Phys.* 52, 153001 (2019).
https://doi.org/10.1088/1361-6463/aafd0b
Google Scholar Crossref

12. K. K. Amireddy, K. Balasubramaniam, and P. Rajagopal, *Appl. Phys. Lett.* 108, 224101 (2016).
https://doi.org/10.1063/1.4950967
Google Scholar Crossref

13. P. Ray, X. Yu, Z. Fan, B. Srinivasan, and P. Rajagopal, *Smart Mater. Struct.* 28(8), 085026 (2019).
https://doi.org/10.1088/1361-665x/ab2e36
Google Scholar Crossref

14. S. A. Cummer, J. Christensen, and A. Alù, *Nat. Rev. Mater.* 1(3), 16001 (2016).
https://doi.org/10.1038/natrevmats.2016.1
Google Scholar Crossref

15. J.-Y. Ou, E. Plum, and N. I. Zheludev, *Appl. Phys. Lett.* 113, 081104 (2018).
https://doi.org/10.1063/1.5036966
Google Scholar Crossref

16. A. Banerjee, R. Das, and E. P. Calius, *Arch. Comput. Methods Eng.* 26(4), 1029–1058 (2019).
https://doi.org/10.1007/s11831-018-9268-1
Google Scholar Crossref

17. K. K. Amireddy, K. Balasubramaniam, and P. Rajagopal, *Sci. Rep.* 7(1), 7777 (2017).
https://doi.org/10.1038/s41598-017-08036-4
Google Scholar Crossref
PubMed

18. K. K. Amireddy, K. Balasubramaniam, and P. Rajagopal, *Appl. Phys. Lett.* 113, 124102 (2018).
https://doi.org/10.1063/1.5045087
Google Scholar Crossref

19. S. A. R. Kuchibhatla and P. Rajagopal, *NDT&E Int.* 102, 304–310 (2019).
https://doi.org/10.1016/j.ndteint.2019.01.006
Google Scholar Crossref

20. C. T. Manjunath and P. Rajagopal, *Sci. Rep.* 9, 6368 (2019).
https://doi.org/10.1038/s41598-019-42655-3
Google Scholar Crossref
PubMed

21. L. Ferrari, C. Wu, D. Lepage, X. Zhang, and Z. Liu, *Prog. Quantum Electron.* 40, 1–40 (2015).
https://doi.org/10.1016/j.pquantelec.2014.10.001
Google Scholar Crossref

22. Z. He, F. Zheng, Y. Ma, H. H. Kim, Q. Zhou, and K. K. Shung, *J. Acoust. Soc. Am.* 137(5), 2785–2790 (2015).
https://doi.org/10.1121/1.4919318
Google Scholar Crossref
PubMed

23. F. Hong and R. Blaikie, *Adv. Opt. Mat.*, 7 1801653 (2019).

https://doi.org/10.1002/adom.201801653
Google Scholar Crossref

24. N. Kaina, F. Lemoult, M. Fink, and G. Lerosey, *Nature* 525, 77 (2015).
https://doi.org/10.1038/nature14678
Google Scholar Crossref
PubMed